Fusion of Satellite and UAV Imagery for Crop Monitoring

Ayyappa Reddy Allu[1] , Shashi Mesapam[1]

[1] Department of Civil Engineering, National Institute of Technology, Warangal, India – (aa721015@student.nitw.ac.in, mshashi@nitw.ac.in)

Keywords: Crop Monitoring, Image Fusion, Satellite Imagery, Unmanned Aerial Vehicle (UAV), Vegetation Indices.

Abstract

Crop monitoring is crucial for precision agriculture, providing insights for optimizing yield and managing resources effectively. This study explores the fusion of Unmanned Aerial Vehicle (UAV) and Sentinel-2 (S2) satellite imagery for monitoring the crop by analyzing vegetation indices and canopy height information from the temporal dataset. Brovey Transform (BT) and Principal Component Analysis (PCA) fusion techniques are used to fuse the UAV and satellite images, aiming to leverage the high spatial resolution of UAV imagery with the broader spectral range of S2 data. Five key vegetation indices, including NDVI, GNDVI, SAVI, EVI, and LAI, were calculated from UAV, S2, and fused imagery in various temporal dates. Canopy height was derived from UAV data, and statistical analyses, including coefficient of determination (R^2), Pearson correlation coefficient, and Root Mean Square Error (RMSE), were performed to assess relationships between canopy height and vegetation indices across the fused images and UAV and S2 images. Results indicate that fused imagery significantly enhances crop health metrics' accuracy and spatial relevance, with high R^2 values and strong correlations between vegetation indices of fused images and UAV images, suggesting enhanced predictive power in monitoring crop health. Our findings highlight the advantages of fusing UAV and S2 imagery for comprehensive crop condition assessment, demonstrating that fused images provide a robust tool for monitoring crop vigor and stress levels. This approach offers valuable support for timely, data-driven decisions in crop management practices.

1. Introduction

Crop Monitoring is essential for maintaining and enhancing agricultural productivity, ensuring food security, and managing resources efficiently. By continuously assessing crop health, farmers and agronomists can detect early signs of stress due to factors like nutrient deficiencies, water scarcity, pests, and diseases (Ahmad et al., 2022). Early detection allows for timely intervention, reducing potential losses and minimizing the need for costly inputs. Crop health here resources such as water, fertilizers, and pesticides are applied selectively, and optimizing crop yield while reducing environmental impact (G & Rajamohan, 2022).

Satellite data has become a valuable tool for monitoring crop parameters, leveraging a range of multispectral, hyperspectral, and thermal sensors on satellites to capture large-scale information about vegetation (Rembold et al., 2015). Satellite data provide indices for monitoring of crop parameters such as growth, chlorophyll content, moisture levels, stress detection, and even some aspects of nutrient deficiencies across wide areas, offering insights that are particularly useful for large-scale agriculture. Despite these advantages, satellite-based crop monitoring faces notable limitations. Spatial resolution can be inadequate for small or mixed-crop fields, where fine-grained detail is necessary. Atmospheric interference, such as clouds or haze, further limits data quality and availability, making it challenging to obtain consistent information over time. These limitations highlight the need for complementary technologies, such as UAVs and ground sensors, to provide more detailed, frequent, and reliable crop data (Sishodia et al., 2020).

UAV equipped with high-resolution sensors provide valuable insights into plant health by measuring indicator allowing farmers to monitor variations in crop growth and detect early signs of stress (Zhao et al., 2019). Data processing techniques, including machine learning algorithms and vegetation indices are commonly used to analyse the imagery, providing actionable information on crop at a field scale. However, despite their benefits, the high cost of UAV equipment and sensors can be prohibitive for many small-scale farmers (Ayyappa Reddy & Shashi, 2023).

Image fusion technology helps to combining the data from various sources such as satellites, UAVs and ground sensors. The integration of UAV and satellite data has significantly advanced agricultural monitoring and stress detection (Allu & Mesapam, 2024a). Various studies highlight the potential of multispectral data fusion in characterizing crop health and optimizing field management practices. UAV integrated sensors combined with satellite data could pre-emptively identify stress development in soybean crops, allowing for proactive irrigation scheduling and enhanced yield outcomes. They employed temporal fusion techniques using indices such as NDVI, NDRE, and GNDVI, achieving improved accuracy in detecting moderate to severe water stress, underscoring the importance of timely intervention in crop management (Sagan et al., 2019).

The fusion of UAV and satellite imagery not only improved the accuracy of vegetation classification but also provided methodological support for agricultural resource surveys (Zou et al., (2018). This advancement facilitates a more refined approach to precision agriculture, as higher classification performance allows for better discrimination between crop types and health statuses. Li et al., (2022) introduced a spatiotemporal fusion framework, STARFM that enhanced the monitoring of winter wheat growth by effectively harmonizing UAV and satellite imagery. Their results indicated that this approach significantly improved the spectral and spatial fusion effects, demonstrating the capability of integrated remote sensing data to provide more detailed insights into crop growth dynamics.

Moreover, the combination of UAV imagery with satellite data has proven beneficial for various agricultural applications, including soil salinity mapping and crop classification. Ma et al., (2020) utilized spectral index fusion techniques to enhance the accuracy of salinity assessments in coastal areas by merging

UAV and Sentinel-2 imagery. This integration facilitated a more detailed understanding of soil conditions affecting crop health. Similarly, Zhao et al., (2019) reported significant improvements in classification accuracy when fusing UAV images with Sentinel-2A data, showcasing how multispectral data fusion can optimize agricultural monitoring and resource management. Overall, the advancements in UAV and satellite data integration present a promising avenue for enhancing agricultural productivity and sustainability through improved monitoring techniques.

From the previous literature Allu & Mesapam, (2024a, 2024b), suggested to fuse the Red band of UAV imagery with the satellite image using the BT and PCA fusion techniques to generate the high spatial and spectral imagery with minimal spatial and spectral distortions and these images produce high classification accuracy imageries compared to the other band combinations and fusion techniques.

The main aim of the study is to monitor the crop parameters using the fused images of satellite and UAV imagery using BT and PCA fusion techniques. In this work, Red band of UAV image is fused with the multispectral imagery of satellite to generate the high spatial and spectral images in various temporal dates. Five vegetation indices are generated from the UAV, S2 and fused images and canopy height from UAV imagery are compared with each other to identify the efficacy of the fusion images in monitoring the crop.

2. Study Area

The study area is situated in Dharmasagar, a region within the Warangal district of Telangana, India (Fig. 1). This area is geographically located at the coordinates 17°59'54" latitude and 79°26'53"E longitude, providing a warm and semi-arid climate suitable for various agricultural practices.

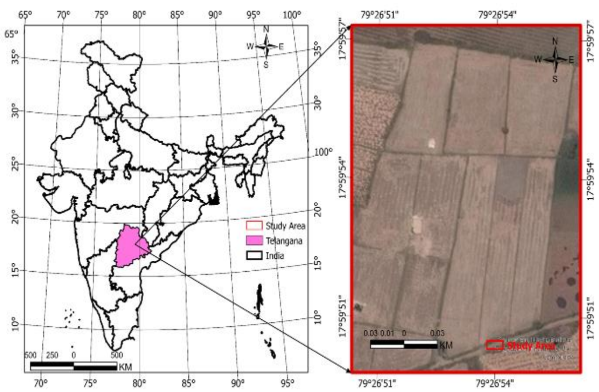

Figure 1. Study Area

Paddy and maize are the primary crops cultivated in Dharmasagar, reflecting the region's reliance on staple food crops that are well-suited to the local climatic and soil conditions. The cultivation cycle here is heavily dependent on groundwater for irrigation. In this study area, paddy crop is cultivated at the time of data collection.

3. Methodology

The methodology for monitoring the crop parameters using the fused images are presented in the fig. 2.

3.1 Data Collection

3.1.1 Satellite Imagery

Satellite images from Sentinel–2 were obtained from the Copernicus Browser (https://browser.dataspace.copernicus.eu/) website. S2 multispectral imaging mission has 13 multispectral bands with a spatial resolution of 10m, 20m, and 60m and the revisit frequency of the satellite is 5 days at the equator. The cloud cover percentage of the collected temporal S2 products are presented in Table 1.

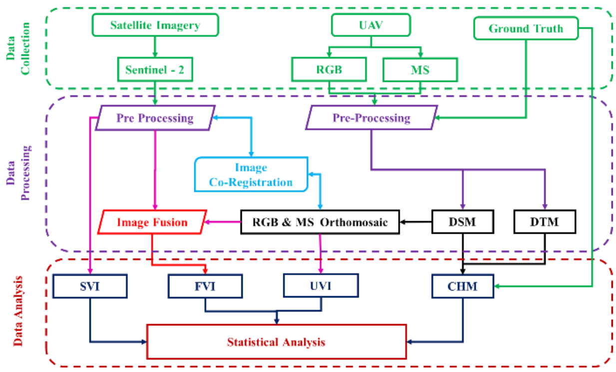

Figure 2. Methodology flowchart of crop monitoring using the fusional images

3.1.2 UAV Imagery

In order to capture crop information on the same day as the S2 images, UAV survey was conducted. Aerial images of crops in the study area were acquired with 5 day interval from March 03, 2024 to April 27, 2024 with ideaForge Q4i (https://ideaforgetech.com/security-and-surveillance/q4i-uav) equipped with Parrot SEQUOIA+ Multispectral (MS) Sensor. The MS sensor captured the images in four narrow bands (Green (550nm±40nm), Red (660nm±40nm), Red Edge (735nm±10nm), and Near Infrared (NIR) (790nm±40nm)) along with one RGB (Red, Green, and Blue) sensor. Narrow bands are captured with 1.2MP camera and RGB images are captured with 16MP camera. The UAV was flown at an altitude of 60m with the camera facing the centre at a 90° to the horizontal and maintaining 80% overlap between the images. The UAV's speed was set to 7 m/s during image capture. The UAV flight path was planned using the BlueFire Touch Ground Control Station.

3.1.3 Ground Truth

Canopy height information is collected from the field using the Differential Global Positioning System (DGPS) equipment and measuring scale. DGPS equipment used to collect the latitude, longitude and elevation of ground position and measuring scale is used to collect the actual canopy height in the field.

3.2 Data Processing

3.2.1 Satellite Imagery

Sentinel-2A L1C Top of Atmosphere (TOA) products are indeed orthorectified and spatially registered products are corrected for radiometric and geometric errors but not corrected for atmospheric errors, such as absorption, and scattering. The SEN2COR atmospheric correction algorithm was used for correct TOA reflectance data to surface reflectance. This correction accounts for the scattering of air molecules, the effects of atmospheric gases, and the absorption and scattering of aerosol particles. The pre-processed bands of the S2 products were layer stacked and developed with a spatial resolution of 10m.

3.2.2 UAV Imagery

MS sensor captured separate images for each spectral band in Tagged Image File Format (.tiff) and RGB image in Joint Photographic Experts Group (.JPEG) format. Collected UAV imageries are encrypted with the information of camera positions (i.e. latitude, longitude, and elevation) which are acquired by GPS and attitude parameters such as omega, phi and kappa are acquired by Inertial Measurement Unit (IMU) of the UAV. These camera positions were used to determine the coordinates of the imagery location including the UAV’s roll, yaw, and pitch movements. The images were then aligned based on inertial measurements using the ground control points established using GPS. Once the images were aligned, tie points were generated from the common points between the images, which were used to orient the images. A mesh is generated by reconstructing the model using the tie points extracted from the images. Point cloud was generated using the tie points of the imagery and which is used to generate the Digital Surface Model (DSM), Digital Terrain Model (DTM), orthomosaic images of RGB and MS. The spatial resolutions of the generated UAV images are presented in Table 1.

Day of the Year (DOY)	UAV Image Resolution (cm/pixel)		S2
	RGB	MS, DEM and DTM	Cloud Cover (%)
03/03/2024	2.24	7.74	0.00
08/03/2024	1.65	5.77	2.50
13/02/2024	1.86	6.41	9.75
18/03/2024	1.74	6.08	74.57
23/03/2024	1.76	6.10	0.00
28/03/2024	1.71	6.00	0.00
02/04/2024	1.75	6.12	7.37
07/04/2024	1.79	6.14	16.77
12/04/2024	1.75	6.22	42.96
27/04/2024	1.72	5.96	0.00

Table 1. Specifications of the UAV and S2 imagery

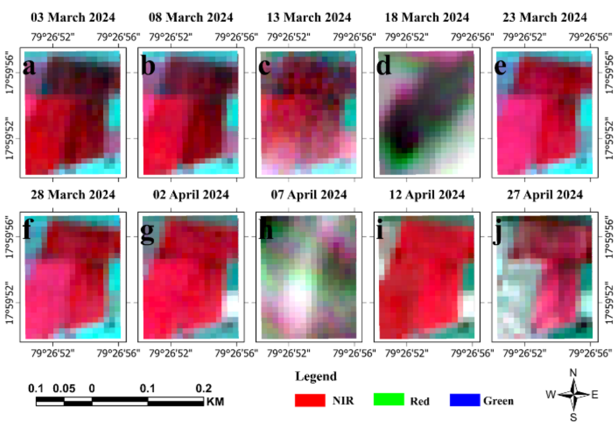

Figure 3. Co-registered layer stacked S2 images

The generated UAV images are resampled to 6 cm/pixel for maintaining the consistency between the images. The pre-processed S2 and UAV images are co-registered with each other before performing the image fusion operation. The co-registered images of the layer stacked S2 products and corresponding UAV RGB and MS orthomosaic images of the various Day of the Year (DOY) are presented in fig. 3, 4, and 5 respectively.

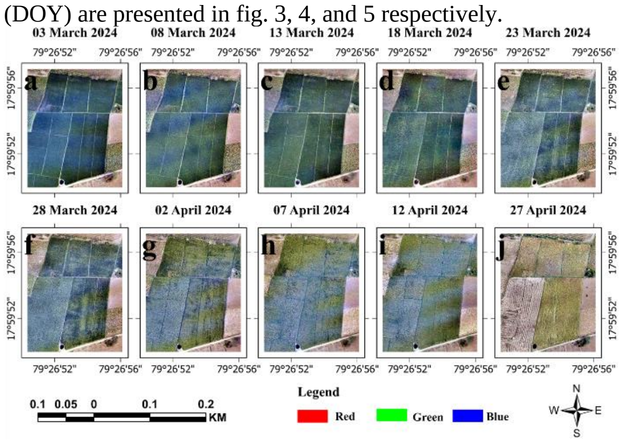

Figure 4. Temporal UAV RGB orthomosaic images

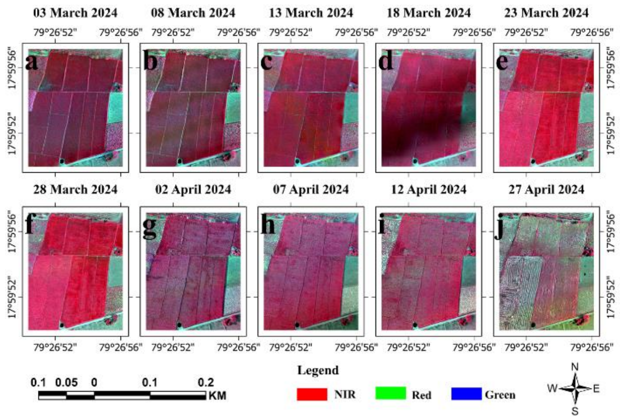

Figure 5. Temporal UAV MS orthomosaic images

3.2.3 Image Fusion: BT and PCA fusion techniques were used in this study to fuse the Red band of UAV imagery with the multispectral imagery of S2.

Brovey Transformation Fusion

The BT enhances spatial resolution by incorporating high-resolution UAV data with multispectral S2 data (Dadrass Javan et al., 2021; Ha et al., 2013). Step by step procedure of fusion of satellite and UAV imagery using BT fusion technique is explained below (Eq. (1) – (3)):

i. Resample the UAV band’s spatial resolution to match the coarser S2 image resolution, ensuring compatibility for pixel-by-pixel fusion.
ii. For each pixel, calculate the Brovey Ratio (BR), which represents the relative contribution of UAV data compared to the combined UAV and S2 values.

$$BR(x,y) = \frac{UAV(x,y)}{S2(x,y)+UAV(x,y)}, \quad (1)$$

iii. Scale the Brovey Ratio so that values fall between 0 and 1, normalizing them based on the maximum pixel value.

$$BR_{norm}(x,y) = \frac{BR(x,y)}{max(BR)}, \quad (2)$$

iv. Combine the normalized Brovey Ratio with the high-resolution image to enhance spatial detail using a linear combination. A weighting factor α determines the proportion of UAV data contribution.

$$F(x,y) = (1-\alpha) \times High(x,y) + \alpha \times UAV(x,y) \times BR_{norm}(x,y) \quad (3)$$

This BT-based fusion method effectively enhances spatial resolution by emphasizing UAV data where it provides the most detail, while retaining the multispectral information of the S2 image.

Principal Component Analysis (PCA) Fusion

The PCA fusion method reduces data dimensionality by transforming the original spectral data into a new set of components, called principal components, which capture most of the information while eliminating redundancy (Metwalli et al., 2009). Step by step procedure of fusion of satellite and UAV imagery using PCA fusion technique is explained below Eq. (4) – (11):

i. Combine the UAV band and S2 image data into a single matrix X with each column representing one dataset.

$$X = [UAV(:), S2(:)] \quad (4)$$

ii. Compute the covariance matrix (C) of X to understand the variance and relationships between the datasets.

$$C = cov(X) \quad (5)$$

iii. Calculate the eigenvectors and eigenvalues of C, where the eigenvectors represent the directions of maximum variance in the data.

$$[V, D] = eig(C) \quad (6)$$

iv. Select the first K eigenvectors (P) that capture most important information from eigenvectors and eigenvalues.

v.

$$P = V(:, 1{:}K) \quad (7)$$

vi. Transform the high resolution (UAV) and low-resolution images (S2) into the PCA space using the matrix P.

$$UAV_{PCA} = P' \times UAV(:) \quad (8)$$

$$S2_{PCA} = P' \times S2(:) \quad (9)$$

vii. Average the transformed components from UAV and S2 data to create a fused component.

$$F_{PCA} = \frac{UAV_{PCA} + S2_{PCA}}{2} \quad (10)$$

viii. Finally, apply the inverse transformation to convert the fused PCA components back into the original image space, creating the fused image with enhanced spectral detail.

$$F = reshape(P \times F_{PCA}, size(UAV)) \quad (11)$$

This PCA-based fusion efficiently combines spectral information from UAV and S2 images, balancing resolution and spectral detail.

3.3 Data Analysis

3.3.1 Vegetation Index

Five vegetation indices are calculated from the S2 (SVI), UAV (UVI) and fused images (FVI). These vegetation indices are very helpful for monitor the crop parameters.

Indices	Formula	Application	Ref.
Normalized Difference Vegetation Index (NDVI)	$\frac{NIR - Red}{NIR + Red}$	Monitor the growth and health of vegetation and to identify areas of stress or damage	(Jiang et al., 2021)
Green Normalized Difference Vegetation Index (GNDVI)	$\frac{NIR - Green}{NIR + Green}$	Estimate chlorophyll content in leaves, making it useful for assessing nitrogen levels and photosynthetic activity in crops.	(Mangewa et al., 2022)
Soil Adjusted Vegetation Index (SAVI)	$\frac{NIR - Red}{NIR + Red + L} \times (1 + L)$	Evaluate vegetation health in areas with sparse vegetation, as it adjusts for soil brightness to provide a clearer indication of plant condition in soil-influenced environments	(Huete, 1988)
Enhanced Vegetation Index (EVI)	$2.5 \times \frac{NIR - Red}{NIR + 6 \times Red - 7.5 \times Blue + 1}$	Monitoring crop canopy structure and biomass	(Sishodia et al., 2020)
Leaf Area index (LAI)	$3.618 \times EVI - 0.118$	Estimations of crop growth, canopy density, and potential photosynthetic activity	(Boegh et al., 2002)

Table 2. Vegetation indices used for monitoring the crop parameters

3.3.2 Canopy Height Model (CHM)

CHM derived from UAV data is a valuable tool for assessing crop growth and overall plant health. CHMs are generated by from Digital Terrain Model (DTM), which represents the bare earth surface, from a Digital Surface Model (DSM) that includes all surface features such as vegetation, buildings, and other objects. The difference between the DSM and DTM represents the height of the vegetation canopy above ground level and the equation is expressed in Eq. (12). This model enables researchers to monitor plant growth dynamics, detect areas with stunted growth, and assess crop parameters by correlating canopy height with plant vigor and yield potential (de Castro et al., 2021). The CHM is particularly useful in precision agriculture, as it provides spatially detailed height measurements that can support targeted interventions, helping optimize crop management practices based on real-time plant height variability within fields.

$$CHM = DSM - DTM \quad (12)$$

This contribution has been peer-reviewed. The double-blind peer-review was conducted on the basis of the full paper.
https://doi.org/10.5194/isprs-annals-X-G-2025-71-2025

3.3.3 Statistical Analysis

Statistical analysis plays a crucial role in evaluating the accuracy and effectiveness of the fused imagery compared to the UAV and S2 imagery for monitoring the crop parameters. For performing the statistical analysis, data was extracted from the 20 known location points from each dataset using R Studio software. Three common statistical metrics used in this context are Root Mean Square Error, Pearson correlation coefficient, and the coefficient of determination.

RMSE is a widely used metric that quantifies the differences between the indices of UAV, S2 and fused images (Ma et al., 2020). RMSE is calculated using the formula (Eq. (13)):

$$RMSE = \sqrt{\frac{\sum_{i=1}^{n}(x_i - \bar{x}_i)^2}{n}} \tag{13}$$

where x_i represents the observed values, $\bar{x}_i$ are the predicted values, and n is the total number of observations. A lower RMSE value indicates a better fit between the predicted and observed values, thus demonstrating the model's accuracy in estimating crop parameters such as chlorophyll content, moisture levels.

Pearson correlation coefficient measures the linear correlation between two variables, indicating how closely the relationship aligns with a straight line (Somvanshi & Kumari, 2020). The formula for the Pearson coefficient (r) is expressed in Eq. (14):

$$r = \frac{\sum_{i=1}^{n}(x_i - \bar{x})(y_i - \bar{y})}{\sqrt{\sum_{i=1}^{n}(x_i - \bar{x})^2}\sqrt{\sum_{i=1}^{n}(y_i - \bar{y})^2}} \tag{14}$$

In this equation, x_i and y_i are the individual sample points, and $\bar{x}$ and $\bar{y}$ are the means of the respective datasets. The Pearson coefficient ranges from -1 to 1, where values closer to 1 indicate a strong positive correlation, values near -1 indicate a strong negative correlation, and values around 0 suggest no correlation.

The **coefficient of determination** is another essential statistical measure that provides insight into how well the independent variable(s) explain the variability of the dependent variable (Mangewa et al., 2022). R^2 is calculated as follows (Eq. (15):

$$R^2 = 1 - \frac{\sum_{i=1}^{n}(y_i - \bar{y}_i)^2}{\sum_{i=1}^{n}(y_i - \bar{y})^2} \tag{15}$$

R^2 values range from 0 to 1, with values closer to 1 indicating that a significant proportion of the variability in the dependent variable is explained by the model. In the context of crop monitoring, a high R^2 value would imply that the fusion of satellite and UAV data effectively captures the variation in crop parameters, reinforcing the model's predictive power.

Together, RMSE, Pearson correlation coefficient, and R^2 provide a comprehensive framework for assessing the accuracy and reliability of crop monitoring using fused remote sensing data. By applying these statistical analyses, researchers can validate efficiency of the fused images for monitoring the crop parameters compared to the UAV and S2 images.

4. Results and Discussions

Fusion of UAV and S2 imagery using the BT and PCA fusion techniques are generated multispectral imagery with a spatial resolution of 6cm/pixel. Fused images of BT and PCA fusion techniques are presented in fig. 6 and 7 respectively.

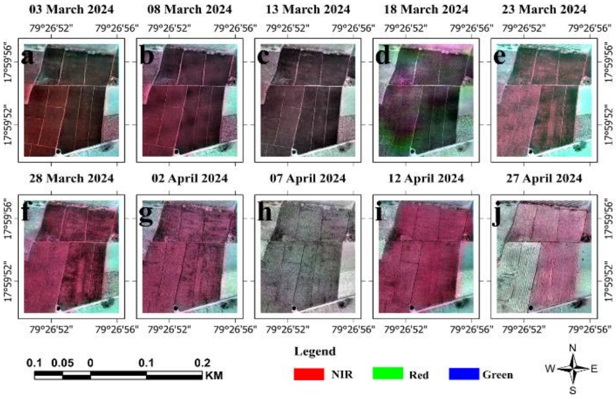

Figure 6. Temporal BT fused images

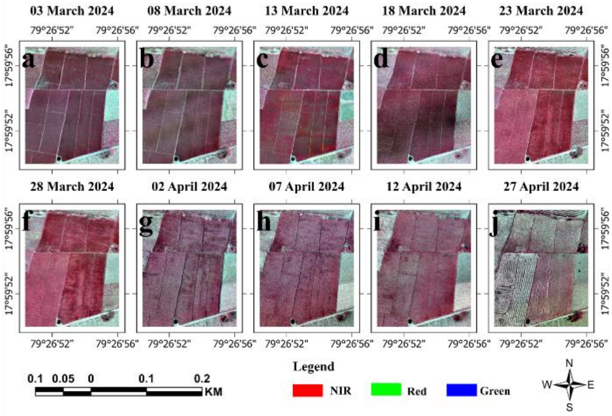

Figure 7. Temporal PCA fused images

Vegetation indices: VI's were calculated from the UAV, S2 and fused imagery for the various temporal dates. The mean values of the indices were presented in the fig. 8.

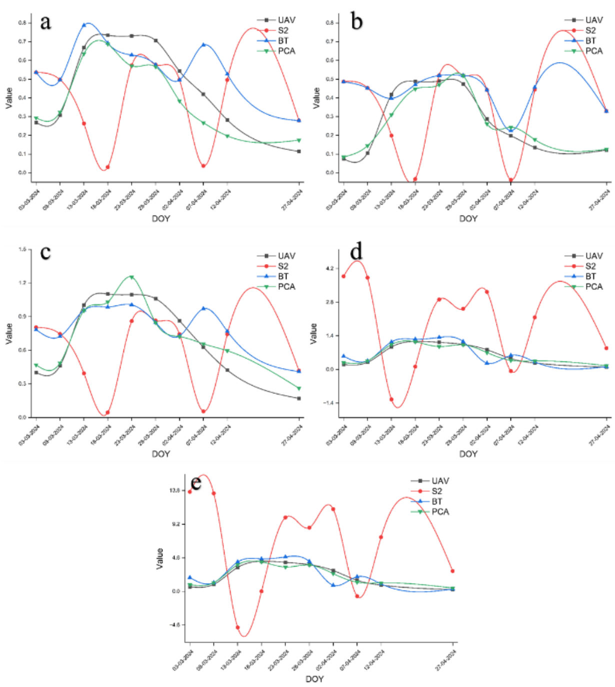

Figure 8. Mean values of vegetation indices of the various temporal dates: a) NDVI, b) GNDVI; c) SAVI; d) EVI; e) LAI

From the fig. 8, the mean values of the vegetation indices from fused images of BT and PCA are nearly coinciding with the mean values of VI from the UAV images but the mean values of VI from the S2 images are fluctuating may be the reason due to coverage of large area information in a single pixel.

For the NDVI, UAV and PCA fused images provided the slightly lower values on some dates, and BT often records higher values. UAV, specifically, has the highest NDVI on March 18, 2024, suggesting UAV images might capture a more intense vegetation signal during peak growth periods. The GNDVI values of the PCA fused images are tend to align closely with UAV measurements, especially in early March, reflecting consistency in vegetation reflectance.

For SAVI, UAV shows consistently higher values, particularly on March 18, 2024, indicating its potential to capture finer soil-adjusted vegetation signals. BT values tend to align with UAV but are slightly lower, while S2 shows significant variations, suggesting that S2 might record lower soil-adjusted vegetation activity in some instances compared to UAV. PCA generally reflects moderate SAVI values, bridging the gap between UAV and S2.

UAV and BT fused images shows that, they closely aligned LAI values across dates, capturing consistent canopy growth over time. PCA values generally fall between UAV and BT values but remain consistently lower than S2, providing an alternative moderate interpretation of leaf area density. UAV and fused images of BT and PCA datasets exhibit closer consistency, while S2 shows greater variability and potentially captures extreme vegetation signals across indices.

Canopy Height: CH of the paddy crop on various temporal dates was extracted from the UAV canopy height model. The median and distribution of canopy height values in different temporal dates are represented in the violin plot (fig. 9).

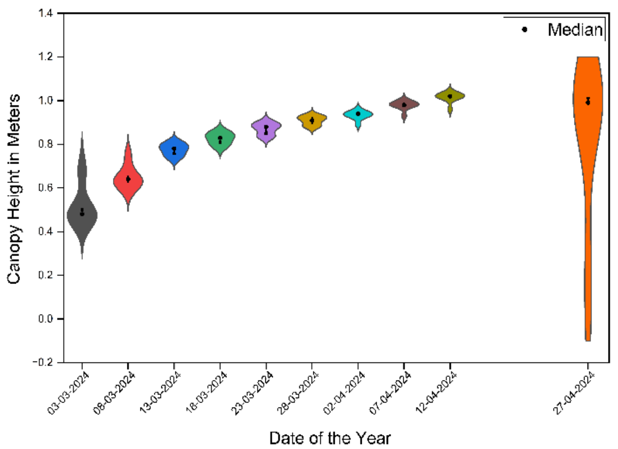

Figure 9. Violin plot of canopy height values of paddy crop in various temporal dates

The scatter plot between the measured canopy height (from UAV-derived data) and the field-measured canopy height reveals a strong linear relationship, as indicated by the linear regression equation which is indicated in fig. 10. This equation suggests a close approximation between UAV-derived and field-measured values, with a slope of 0.94 and a small positive intercept (0.03), indicating that the UAV-measured canopy height estimates are slightly lower on average than the field measurements but very close to parity. The RMSE of 0.04m further supports the accuracy of the UAV measurements, as it reflects minimal deviation from field values. The high (R^2) suggests that 95% of the variation in measured canopy height can be explained by the field measurements, highlighting the effectiveness of UAV-based methods in estimating canopy height with high fidelity.

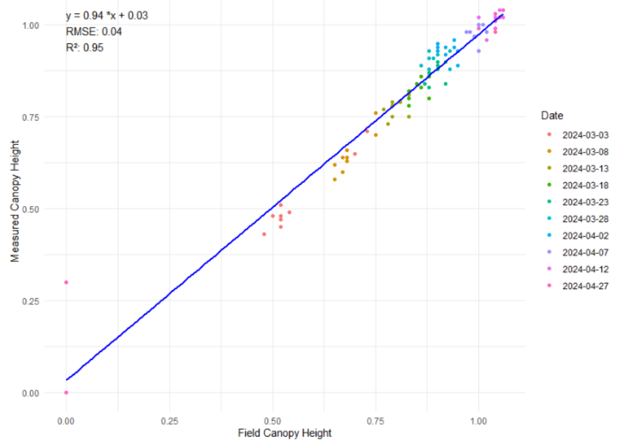

Figure 10. Scatter plot between measured and field canopy height

The statistical analysis is performed between the extracted information from the vegetation indices of UAV, S2 and fused images of UAV and S2. The results indicate significant variations in RMSE values (fig. 11), revealing insights into the effectiveness and limitations of each imagery source and fusion technique. UAV Imagery consistently presented low RMSE values across different indices, such as UAV_NDVI vs. UAV_SAVI and UAV_NDVI vs. UAV_GNDVI underscoring its high precision and suitability for detailed crop analysis. However, UAV based measurements of LAI exhibited slightly higher RMSE values when compared with other indices, which may reflect the challenges in capturing leaf area accurately at smaller scales with UAVs alone. S2 imagery alone showed relatively higher RMSE values for maximum combinations, Larger RMSE values were observed in combinations involving S2_LAI, indicating limitations in its capacity to accurately capture certain crop biophysical characteristics when compared to high-resolution UAV imagery.

Brovey Transform (BT) Fusion yielded the lowest RMSE between indices for certain pairs, such as BT_EVI (EVI index from the BT fused image) Vs. BT_LAI, indicating high consistency between these indices in fused imagery. This suggests that BT fusion effectively harmonizes vegetation indices, making it highly reliable for crop monitoring. Conversely, PCA fusion exhibits a slightly higher RMSE for similar index comparisons, such as PCA_EVI and PCA_LAI, indicating minor discrepancies between indices within PCA-fused images.

The analysis indicates that BT fusion provides more stable and reliable vegetation index measurements for crop monitoring than standalone UAV or Sentinel-2 imagery. Fused BT imagery achieves lower RMSEs across most index comparisons, suggesting it can offer more consistent and precise insights into crop health. PCA fusion, while beneficial, exhibits slightly higher RMSEs, indicating less reliability in harmonizing certain indices compared to BT fusion.

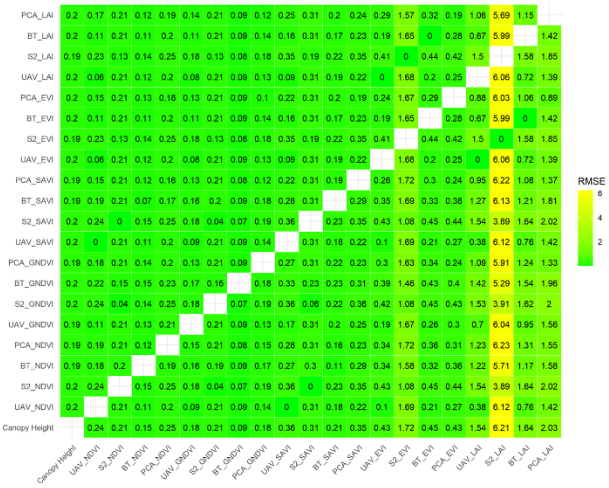

Figure 11. Heat map of RMSE values between the UVI, SVI, FVI and canopy height

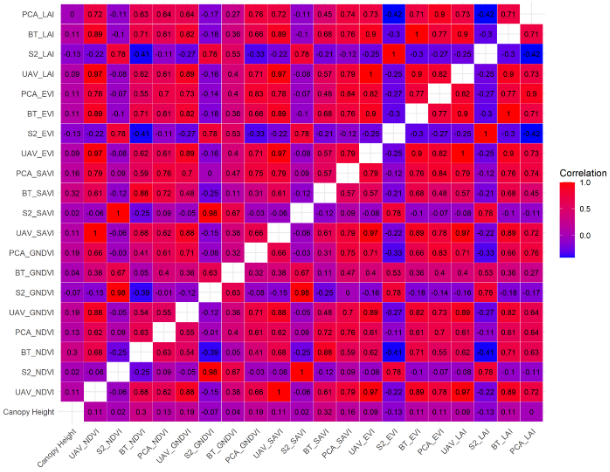

Figure 12. Heat map of Pearson Correlation Coefficient values between the UVI, SVI, FVI and canopy height

The comparison of vegetation indices derived from UAV, S2, and fused images of BT and PCA fusion techniques demonstrates significant correlations between the images and it is represented in the fig. 12. Pearson correlation values of the images provide insights into the effectiveness of each imaging technique for field crop monitoring. High Pearson correlation coefficients ($r > 0.9$) were observed among certain indices within the same imaging source, such as UAV NDVI, UAV SAVI, S2 NDVI, S2 SAVI, BT EVI and BT LAI. These strong correlations suggest that within individual data sources, certain indices respond similarly to crop characteristics, implying reliable consistency within UAV, S2, and fused datasets for these specific index pairs.

The fused images of BT and PCA are also correlated well with some UAV indices, with notable correlations between BT EVI and UAV indices such as UAV LAI, UAV EVI, and UAV NDVI ($r \approx 0.9$). These findings indicate that fused images, especially those based on BT, can enhance UAV-derived metrics and potentially improve spatial and temporal crop monitoring, leveraging both UAV and satellite data's spatial and spectral advantages.

Moderate correlations ($0.7 < r < 0.8$) appeared between certain UAV indices and PCA-derived indices, with UAV NDVI and PCA EVI ($r = 0.78$) and UAV SAVI and PCA EVI ($r = 0.78$) demonstrating reasonable compatibility. However, these values indicate some level of divergence, suggesting that PCA fusion might capture unique spectral variations not fully aligned with UAV indices.

Lower correlations, particularly among SVI when compared to FVI, point to some limitations in using satellite data alone for high-resolution crop monitoring. For example, correlations between SVI and FVI indices, such as S2 NDVI and PCA SAVI ($r = 0.089$) and S2 LAI and BT LAI ($r = -0.295$), were minimal, highlighting inconsistencies when S2 data is fused with high-resolution sources.

The fusion of UAV and satellite images, especially through BT, offers enhanced correlation and compatibility with UAV indices, suggesting it as a viable method for detailed crop monitoring. However, some indices from PCA fusion showed moderate correlation, and inconsistencies remain when using S2 images alone or compared with fused datasets, emphasizing the need for tailored fusion strategies for optimal index accuracy in crop monitoring.

The analysis of R^2 values between UVI, SVI and FVI are presented in fig. 13 and it provides insights into the effectiveness and comparability of these remote sensing sources and fusion methods in crop monitoring. Indices derived solely from a single platform, such as UAV or S2, generally show strong correlations, with values nearing or equalling 1. For instance, high correlations were observed between BT_EVI and BT_LAI, S2_NDVI and S2_SAVI, and UAV_NDVI and UAV_SAVI, each with an R^2 of 1, indicating strong within-source consistency in monitoring crop parameters.

Comparing vegetation indices between fused images and individual UAV or S2 images reveals some notable findings. The R^2 values for fused BT and UAV data, such as between UAV_NDVI and BT_EVI (0.7899), and between UAV_GNDVI and BT_EVI (0.6662), are moderate, suggesting that fused images offer complementary yet not identical insights compared to single-platform data. Likewise, moderate R^2 values were observed for relationships between UAV and PCA indices, such as UAV_NDVI and PCA_SAVI (0.6186), indicating that while fused indices maintain some alignment with individual UAV indices, they introduce unique information, likely from the added spectral and spatial data.

PCA-based fusion showed slightly lower R^2 values with UAV and S2 data compared to BT fusion, suggesting that BT fusion may better retain individual platform characteristics in the fused imagery. Such results imply that PCA fusion introduces additional variability or perhaps highlights different aspects of crop variability than UAV or S2 indices alone.
The high R^2 values within the UAV and Sentinel-2 data, confirm their effectiveness in capturing consistent crop characteristics. However, fused imagery from BT method, shows promise by moderately aligning with UAV indices while potentially enhancing crop monitoring capabilities through complementary spectral data.

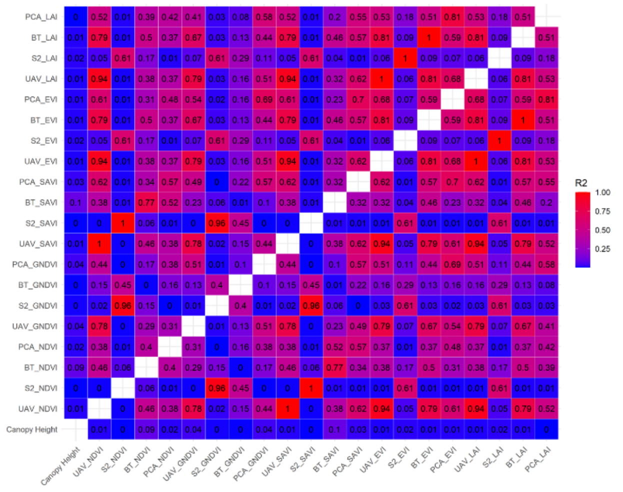

Figure 13. Heat map of R2 values between the UVI, SVI, FVI and canopy height

Overall, the BT fusion method has demonstrated superior performance, achieving more stable and predictable index relationships across datasets. This can be attributed to BT's ability to integrate multi-source spectral bands while minimizing data redundancy, thus improving reliability in vegetation monitoring. The close alignment between indices like EVI and LAI in BT fusion models implies that BT effectively captures and merges the high spatial resolution of UAV with the spectral depth of S2 data, delivering comprehensive, nuanced crop health insights. PCA fusion, while adding value in spectral variance enhancement, presents slightly less consistency in certain index relationships, potentially due to the introduction of mixed spectral components that influence index predictability.

These findings underscore the practical value of fused UAV and S2 imagery for crop monitoring, particularly through BT fusion, which achieves high index reliability and consistency. These advanced fused datasets are promising tools for precision agriculture applications.

5. Conclusion

This study highlights the significant advantages of using fused imagery from UAV and S2 satellites for effective crop health monitoring. The integration of images using both BT and PCA fusion techniques has yielded multispectral data with high spatial resolution (6 cm/pixel), enabling precise canopy height estimations. The strong linear correlation between UAV-derived and field-measured canopy heights, reflected by an RMSE of only 0.04m and a coefficient of determination (R^2) of 0.95, demonstrates the reliability of UAV data in capturing crucial plant height metrics. These findings affirm that UAV-derived canopy height can play a vital role in supporting crop health assessments, yield estimations, and precision agriculture strategies, providing actionable insights for farmers and agricultural managers.

Moreover, the statistical analysis of vegetation indices reveals that BT fusion consistently outperforms PCA fusion in generating reliable and predictable relationships among various vegetation indices. The perfect correlations achieved between BT-derived EVI and LAI underscore the effectiveness of BT fusion in enhancing the predictive capacity of vegetation indices by mitigating noise and capturing multi-spectral information efficiently. Although PCA fusion also offers valuable enhancements, it exhibits slightly lower correlation strength in certain index pairs, indicating potential variability. Overall, these results advocate for the application of fused UAV and S2 imagery as a robust tool for crop health monitoring, contributing significantly to the realm of precision agriculture by ensuring accurate and scalable assessments essential for informed decision-making in agricultural practices.

References

Ahmad, U., Nasirahmadi, A., Hensel, O., & Marino, S., 2022. Technology and Data Fusion Methods to Enhance Site-Specific Crop Monitoring. *Agronomy*, 12(3), 555. https://doi.org/10.3390/agronomy12030555

Akbar Hossain, K., Masiero, M., Pirotti, F., 2022. Land cover change across 45 years in the world's largest mangrove forest (Sundarbans): the contribution of remote sensing in forest monitoring. *European Journal of Remote Sensing* 1–17. https://doi.org/10.1080/22797254.2022.2097450

Allu, A. R., & Mesapam, S., 2024a. Fusion of different multispectral band combinations of Sentinel-2A with UAV imagery for crop classification. *Journal of Applied Remote Sensing*, 18(01). https://doi.org/10.1117/1.JRS.18.016511

Allu, A. R., & Mesapam, S., 2024b. Selection of suitable fusional band combination from Sentinel-2A and UAV imagery for agricultural applications. *Journal of Spatial Science*. https://doi.org/10.1080/14498596.2024.2353158

Ayyappa Reddy, A., & Shashi, M., 2023. IMPACT OF UAV AND SENTINEL-2A IMAGERY FUSION ON VEGETATION INDICES PERFORMANCE. *ISPRS Annals of the Photogrammetry, Remote Sensing and Spatial Information Sciences*, X-1/W1-2023, 785–792. https://doi.org/10.5194/isprs-annals-x-1-w1-2023-785-2023

Boegh, E., Soegaard, H., Broge, N., Hasager, C. B., Jensen, N. O., Schelde, K., & Thomsen, A., 2002. Airborne multispectral data for quantifying leaf area index, nitrogen concentration, and photosynthetic efficiency in agriculture. *Remote Sensing of Environment*, 81(2–3), 179–193. https://doi.org/10.1016/S0034-4257(01)00342-X

Dadrass Javan, F., Samadzadegan, F., Mehravar, S., Toosi, A., Khatami, R., & Stein, A., 2021. A review of image fusion techniques for pan-sharpening of high-resolution satellite imagery. *ISPRS Journal of Photogrammetry and Remote Sensing*, 171, 101–117. https://doi.org/10.1016/j.isprsjprs.2020.11.001

de Castro, A. I., Shi, Y., Maja, J. M., & Peña, J. M., 2021. Uavs for vegetation monitoring: Overview and recent scientific contributions. *Remote Sensing*, 13(11), 1–13. https://doi.org/10.3390/rs13112139

Sharmila, G., & Rajamohan, K., 2022. Image Processing and Artificial Intelligence for Precision Agriculture. *2022 International Conference on Innovative Computing, Intelligent Communication and Smart Electrical Systems (ICSES)*, 1–8. https://doi.org/10.1109/ICSES55317.2022.9914148

Ha, W., Gowda, P. H., & Howell, T. A., 2013. A review of potential image fusion methods for remote sensing-based irrigation management: Part II. *Irrigation Science*, 31(4), 851–869. https://doi.org/10.1007/s00271-012-0340-6

Huete, A. R., 1988. A soil-adjusted vegetation index (SAVI). *Remote Sensing of Environment*, 25(3), 295–309. https://doi.org/10.1016/0034-4257(88)90106-X

Jiang, R., Sanchez-Azofeifa, A., Laakso, K., Wang, P., Xu, Y., Zhou, Z., Luo, X., Lan, Y., Zhao, G., & Chen, X., 2021. UAV-based partially sampling system for rapid NDVI mapping in the evaluation of rice nitrogen use efficiency. *Journal of Cleaner Production*, 289, 125705. https://doi.org/10.1016/j.jclepro.2020.125705

Kanan, A.H., ... Rahman, M.M., 2023. Mapping inundation from sea level rise and its interaction with land cover in the Sundarbans mangrove forest. *Climatic Change* 176, 104. https://doi.org/10.1007/s10584-023-03574-5

Li, Y., Yan, W., An, S., Gao, W., Jia, J., Tao, S., & Wang, W., 2022. A Spatio-Temporal Fusion Framework of UAV and Satellite Imagery for Winter Wheat Growth Monitoring. *Drones*, 7(1), 23. https://doi.org/10.3390/drones7010023

Ma, Y., Chen, H., Zhao, G., Wang, Z., & Wang, D., 2020. Spectral Index Fusion for Salinized Soil Salinity Inversion Using Sentinel-2A and UAV Images in a Coastal Area. *IEEE Access*, 8, 159595–159608.
https://doi.org/10.1109/ACCESS.2020.3020325

Mangewa, L. J., Ndakidemi, P. A., Alward, R. D., Kija, H. K., Bukombe, J. K., Nasolwa, E. R., & Munishi, L. K., 2022. Comparative Assessment of UAV and Sentinel-2 NDVI and GNDVI for Preliminary Diagnosis of Habitat Conditions in Burunge Wildlife Management Area, Tanzania. *Earth (Switzerland)*, 3(3), 769–787. https://doi.org/10.3390/earth3030044

Metwalli, M. R., Nasr, A. H., Farag Allah, O. S., & El-Rabaie, S., 2009. Image fusion based on principal component analysis and high-pass filter. *2009 International Conference on Computer Engineering & Systems*, 63–70. https://doi.org/10.1109/ICCES.2009.5383308

Rembold, F., Meroni, M., Urbano, F., Royer, A., Atzberger, C., Lemoine, G., Eerens, H., & Haesen, D., 2015. Remote sensing time series analysis for crop monitoring with the SPIRITS software: New functionalities and use examples. *Frontiers in Environmental Science*, 3(JUL), 1–11. https://doi.org/10.3389/fenvs.2015.00046

Sagan, V., Maimaitijiang, M., Sidike, P., Maimaitiyiming, M., Erkbol, H., Hartling, S., Peterson, K. T., Peterson, J., Burken, J., & Fritschi, F., 2019. Uav/satellite multiscale data fusion for crop monitoring and early stress detection. *International Archives of the Photogrammetry, Remote Sensing and Spatial Information Sciences - ISPRS Archives*, 42(2/W13), 715–722. https://doi.org/10.5194/isprs-archives-XLII-2-W13-715-2019

Sishodia, R. P., Ray, R. L., & Singh, S. K., 2020. Applications of remote sensing in precision agriculture: A review (Indices vegetativos utilizados na agricultura). *Remote Sensing*, 12(19), 1–31.

Somvanshi, S. S., & Kumari, M., 2020. Comparative analysis of different vegetation indices with respect to atmospheric particulate pollution using sentinel data. *Applied Computing and Geosciences*, 7(June), 100032. https://doi.org/10.1016/j.acags.2020.100032

Zhao, L., Shi, Y., Liu, B., Hovis, C., Duan, Y., & Shi, Z., 2019. Finer classification of crops by fusing UAV images and sentinel-2A data. *Remote Sensing*, 11(24). https://doi.org/10.3390/rs11243012

Zou, Y., Li, G., & Wang, S., 2018. The fusion of satellite and unmanned aerial vehicle (UAV) imagery for improving classification performance. *2018 IEEE International Conference on Information and Automation, ICIA 2018*, *August*, 836–841. https://doi.org/10.1109/ICInfA.2018.8812312